Global and Planetary Change 172 (2019) 200–210

Contents lists available at ScienceDirect

Global and Planetary Change

journal homepage: www.elsevier.com/locate/gloplacha

Research article

Climate-induced discharge variations of the Nile during the Holocene: Evidence from the sediment provenance of Faiyum Basin, north Egypt

Qianli Sun[a,*], Yan Liu[a,*], Alaa Salem[b], Leszek Marks[c], Fabian Welc[d], Fuwei Ma[a], Weiguo Zhang[a], Jing Chen[a], Jun Jiang[a], Zhongyuan Chen[a]

[a] State Key Laboratory of Estuarine and Coastal Research, East China Normal University, Shanghai, 200062, China
[b] Kafrelsheikh University, Faculty of Science, Kafrelsheikh, Egypt
[c] University of Warsaw, Faculty of Geology, Warsaw, Poland
[d] Cardinal Stefan Wyszyñski University, Institute of Archaeology, Warsaw, Poland

ARTICLE INFO

Keywords:
Faiyum Basin
The Nile
Sediment geochemistry
Sediment provenance
Nile discharge

ABSTRACT

The Faiyum Basin of northern Egypt occupies a key location on the source-to-sink pathway of the Nile. High-resolution grain size, organic carbon and carbonates, as well as geochemical and magnetic analyses, were conducted on a sediment core retrieved from the basin to infer changes in sediment provenance in association with climate-induced variations in Nile River discharge during the Holocene. A high Si/Al ratio in the coarse sediment with weak magnetic properties prior to *ca.* 9.7 cal ka BP indicated prevalent aeolian activities in the lake basin, revealing no Nile discharge inputs and thus a dry Nile. Initial high values of the mobile elements (CaO, MgO and Sr) after *ca.* 9.7 cal ka BP with well-sorted finer sediment marked the establishment of a flow connection between the basin and the Nile since then. This establishment was followed by a durative hydrological connection to the Nile until *ca.* 5.0 cal ka BP inferred from high organic matter and stable magnetic and geochemical properties of the finer sediment, implying a humid climate phase of the Nile between *ca.* 9.7–5.0 cal ka BP. Afterwards, an increasing Ti/Al ratio and magnetism of the sediment indicated a brief change in sediment provenance, as material from the volcanic Ethiopian Uplands carried by the Blue Nile and the Atbara became dominant. A drying climate prevailed in the Nile Basin after *ca.* 5.0 cal ka BP. Although the Ti/Al ratio and sediment magnetic properties still showed a prominent sediment contribution from the volcanic Ethiopian Uplands, the natural discharge from the river Nile to the Faiyum Basin was weakened, especially when increasing water extraction by humans occurred after *ca.* 4.0 cal ka BP. The sediment provenance pattern of the Faiyum Basin was substantially influenced by climate-induced variations of the Nile discharge in response to the advance/retreat of the African Summer Monsoon (ASM) driven by the northward/southward migration of the Inter-Tropical Convergence Zone (ITCZ).

1. Introduction

Nile discharge during the Holocene is of particular interest to both paleoclimatic and archaeological communities as it has substantial impacts on the development of African human civilizations (Bubenzer and Riemer, 2007; Welc and Marks, 2014; Macklin and Lewin, 2015; Castañeda et al., 2016). Many studies from the headwaters to the delta and offshore areas with varied sedimentary archives have revealed several distinct periods of hydrological and climatic changes in the Nile basin during the Holocene; they are believed to be associated with variations in the African monsoon, the migration of the Inter-Tropical Convergence Zone (ITCZ) and the El Niño–Southern Oscillation (ENSO) activities on different spatial and temporal scales (Hoelzmann et al., 2001;Stanley et al., 2003;Hamann et al., 2008; Marriner et al., 2012; Marks et al., 2018). Changes in Nile discharge during the Holocene have helped illustrate the interplay between climate forcing and human occupation in the Nile valley and the delta regions (Krom et al., 2002; Kuper and Kröpelin, 2006; Bernhardt et al., 2012). Although investigations have been frequently conducted in the headwater and delta regions of the Nile, there have been limited high-resolution studies carried out on the desert regions of the Nile, where the Nile flows through almost 2700 km of the Sahara Desert without significant perennial tributary inputs. Since the Quaternary, the Nile has been an affluent record of interaction between the desert and the river system

* Corresponding authors.
E-mail addresses: qlsun@sklec.ecnu.edu.cn (Q. Sun), liuyan@sklec.ecnu.edu.cn (Y. Liu).

https://doi.org/10.1016/j.gloplacha.2018.10.005
Received 20 October 2017; Received in revised form 16 August 2018; Accepted 10 October 2018
Available online 10 October 2018
0921-8181/

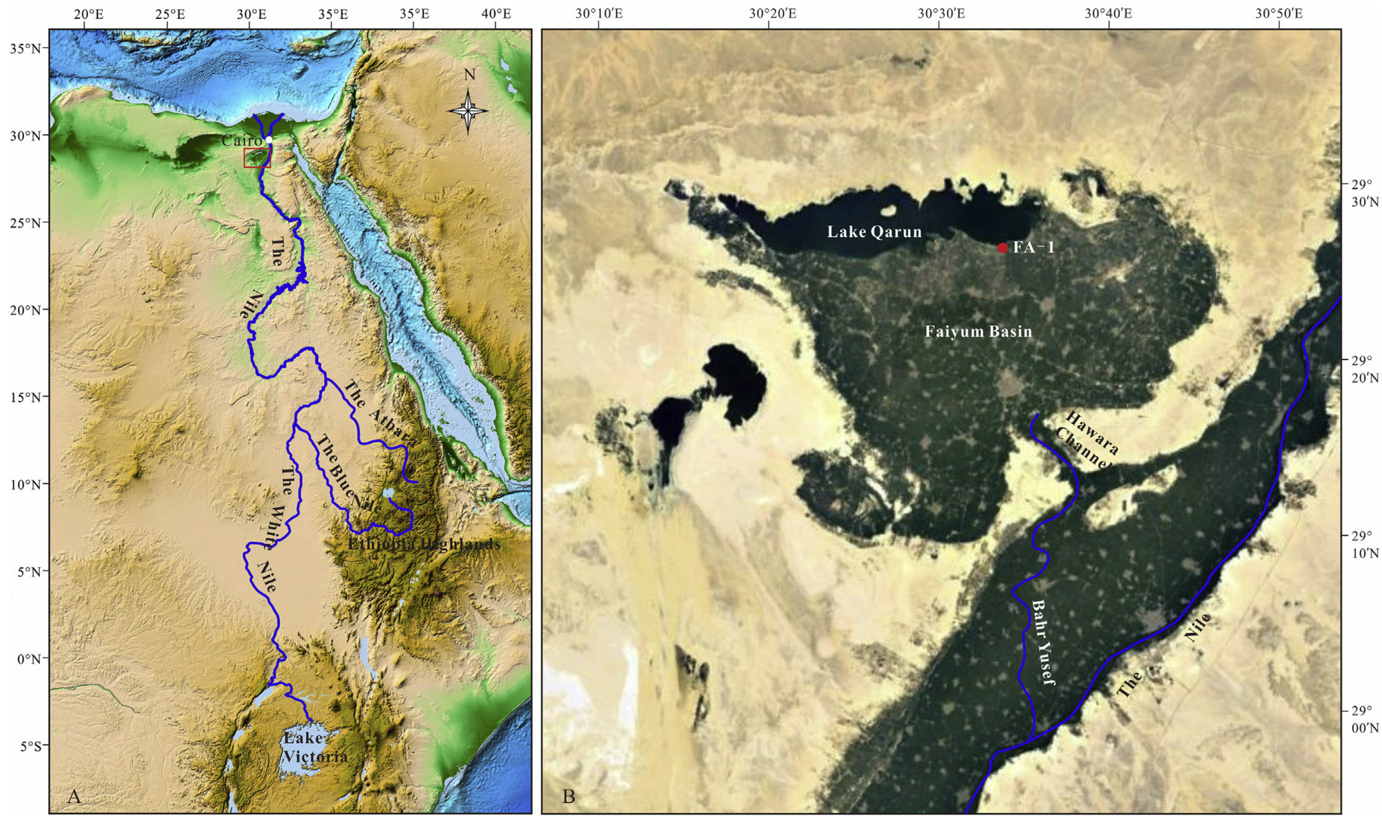

Fig. 1. (A) The Nile River and its catchment, showing the major tributaries of the White Nile, the Blue Nile and the Atbara River (https://www.ngdc.noaa.gov/mgg/global/global.html); (B) the location of core FA-1, Lake Qarun and the Faiyum Basin, also indicated are the Bahr Yusef River and the Hawara Channel. (For interpretation of the references to colour in this figure legend, the reader is referred to the web version of this article.)

over a range of timescales (Stanley et al., 2003; Osborne et al., 2010); Holocene high-resolution environmental records in the desert region of the Nile should be of great significance and provide valuable insights on the interactions between the Nile, environmental change, and human occupations in the hyper-dry region during episodes of different river discharge.

As one of the destinations of Nile material, the Faiyum Basin, is situated at a key location on the source-to-sink pathway of the Nile (Fig. 1). Since the Holocene, the environment of the Faiyum Basin has been influenced by both climate change and hydrological regulations in the Nile catchment (Flower et al., 2006; Kusky et al., 2011; Hassan et al., 2012). Lake Qarun in the Faiyum Basin is one of the very few lakes in the Western Desert of Egypt that contains abundant evidence of early human activities. It originated and survived in the Holocene by virtue of its natural and (later) artificial linkages to the Nile (Hassan, 1986; Flower et al., 2006). Therefore, the sediment of Lake Quran is expected to provide a unique and continuous record of lake basin evolution in the northern desert regions of Egypt in response to the hydro-climate of the Nile catchment during the Holocene.

In the past few decades, studies have been carried out to investigate the evolution of the lake basin in relation to local and east African climate change. Hassan (1986) attributed the Holocene water level fluctuations of Lake Qarun to Nile discharge controlled by sub-Saharan climatic changes. Prehistoric subsistence and settlements around the lake were shaped by both the seasonal Nile water movement and the palaeogeography of the lake. Baioumy et al. (2010, 2011) claimed that the water level changes in Lake Qarun during the last 7000 years was a combination of climate change in the source areas of the Nile, as well as a result of monsoon dynamics, local climate phenomena and human activities. Flower et al. (2012) presented an early-Holocene diatom record with seasonal resolution, which indicated that both the emergence and loss of diatom-rich varves during *ca.* 9935–8693 cal a BP and after that they were closely related to hydrodynamic conditions of the lake resulting from variations in the Nile discharge. There are also some high-resolution studies of the Faiyum Basin based on pollen, foraminifera and sediment magnetic records, but they only cover the recent history of Lake Qarun and the basin (Foster et al., 2008; Hassan et al., 2012). To better understand how the lake basin environment evolved in response to the hydroclimate of the Nile catchment and the forcing dynamics during the entire Holocene, further high-resolution work encompassing multiple approaches is still needed.

The present study is based on a sediment core (FA-1) retrieved from the southern shore of Lake Qarun in the Faiyum Basin (Fig. 1). Grain size, total organic carbon content (TOC), carbonates ($CaCO_3$) and geochemical composition analyses were conducted. In combination with microfossil evidence and the magnetic properties (Jiang et al., 2016), changes in sediment provenance as the lake evolved and its hydrological linkages with the Nile during the Holocene are demonstrated using a radiocarbon dating based chronology. Faiyum Basin and the climate of the Nile Basin in relation to variations in the African Summer Monsoon (ASM) and the migration of the Inter-Tropical Convergence Zone (ITCZ) are discussed at the regional and continental scale.

2. Geological setting

The Faiyum Basin (30° 23′ - 31° 05′ E, 28° 55′ - 29° 35′ N) is located on the north-eastern margin of the Sahara Desert, covering an area of *ca.* 12,000 km^2 (Fig. 1A). The basin is bounded on the north by successive cuesta escarpments, which rise up to approximately 250 m above mean sea level (a.m.s.l) and run in an east-west direction. The outcrops consist of Middle-Upper Eocene limestone, Oligocene clastic and volcano-sedimentary rocks (basalts and pyroclastics) capped by Miocene sandstone near the top of the plateau (Wendorf and Schild, 1976; Said, 1993). A narrow divide, up to 160 m a.m.s.l, separates the depression from the Nile Valley and extends in an NNW to SSE direction. The lower Faiyum Basin is overlain by Quaternary sediments, mainly of lacustrine and aeolian origin (Beadnell, 1905; Said, 1993; Hassan et al., 2012) (Fig. 1). It has been reported that early tectonic movements and enhanced aeolian activity since the Late Pleistocene shaped the lake basin and that the Nile served as the major water source for the basin during the Holocene (Hassan, 1986; Hassan et al., 2012; Baioumy et al., 2010; Kusky et al., 2011).

At present, the Faiyum Basin is hyper-arid with an annual precipitation of *ca.* 7 mm. Rainfall occurs mainly in winter and is carried by N-E trade winds. The average annual temperature is 20.9 °C, while it is an average of 13 °C in winter and 28 °C in summer. The annual drainage and underground water supply to the lake basin are approximately $3.38 \times 10^8\,m^3$ and $0.67 \times 10^8\,m^3$ respectively, while the water loss from evaporation is approximately $4.15 \times 10^8\,m^3$ in total, resulting in an annual net water loss of $0.10 \times 10^8\,m^3$ (Meshal, 1977; El-shabrawy and Dumont, 2009; Tesemma, 2009). The lake water was thought to have occupied most areas of the basin during the Early Holocene, with a maximum level of > 60 m higher than the present, although there were phases with fluctuations (Hassan, 1986). The lake level has fallen gradually since the middle-to-late Holocene as the climate in the Nile Basin has become much drier (Hassan, 1986; Hassan et al., 2012). Today, the water body (Lake Qarun) only exists in the northwest part of the Faiyum Basin at ~44 m below mean sea level, covering an area of *ca.* 200 km^2. The average water depth of the lake is *ca.* 4 m with a maximum depth of *ca.* 8.8 m. The salinity of the lake water is *ca.* 37.6‰ due to high evaporation. Irrigation water flows into the Faiyum depression through the Bahr Yusef canal which connects to the Nile from the east (Fig. 1).

3. Materials and methods

The sediment core FA-1(29° 28′ 07.3“ N, 30° 46′ 44.9” E, ~ − 44 m in elevation) was retrieved in spring of 2014 with a self-propelled American set Acer. The core was collected in a plastic pipe which was 1-m long and 10-cm in diameter, and the total core length was 26.0 m (21.25 m used in the present study) with a recovery rate over 97%. The sampling site was approximately 1.5 m above the present lake level and was covered by artificial accumulations. Therefore, the top 1.9 m was not sampled (Marks et al., 2016, 2018). The rest (1.90–21.25 m) was sampled at a 10 cm interval for grain size, TOC, carbonates, magnetic properties and geochemistry analyses.

3.1. Radiocarbon dating and age-depth model

A total of 32 samples from core FA-1 were selected and dated using an Accelerator Mass Spectrometry (AMS) performed at the Poznań Radiocarbon Laboratory, Poland. The dating materials included terrestrial organic matter, shell detritus and bulk sediment (Marks et al., 2018) (Table 1). The ages were calibrated using the Calib 7.0.1 radiocarbon age calibration program with the INTCAL13 data set and a 95.4% confidence level (2σ); in the present study, ages are expressed either in cal a BP or in cal ka BP (Stueiver and Reimer, 1993; Reimer et al., 2013). The lower part of the core consisted of a sandy deposit and 3 samples with a disordered sequence were dated to the late Pleistocene and were not used for establishing the Holocene chronology. Evident offsets of 6 samples at depths of 5.35, 6.57, 8.05, 8.20, 11.75 and 12.50 m were also excluded. Altogether, 23 dates were used for setting up the age-depth model in the present study. The age-depth pattern was presented using Bacon software (Blaauw and Christen, 2011). The model was determined by setting the core sediments at 10-cm intervals using the statistical software package R (R Development Core Team, 2013).

Table 1
Detailed dating results of Core FA-1.

Lab No.	Depth/m	Material	14C age	Calibrated age (2δ)
Poz-63,658	3.95	Shell detritus	1360 ± 30	1257–1334
Poz-72,534	4.95	Terrestrial organic matter	2395 ± 30	2347–2491
Poz-72,537	5.35	Bulk	1270 ± 30	1173–1287
Poz-68,169	5.55	Bulk	2175 ± 30	2112–2309
Poz-72,521	5.95	Bulk	3210 ± 30	3368–3480
Poz-72,522	6.15	Bulk	2920 ± 30	2969–3160
Poz-64,051	6.67	Terrestrial organic matter	5740 ± 40	6439–6644
Poz-72,523	6.75	Bulk	3500 ± 35	3690–3867
Poz-68,008	7.2	Bulk	3990 ± 60	4247–4620
Poz-72,536	8.05	Bulk	4600 ± 40	5274–5465
Poz-68,007	8.2	Bulk	4540 ± 60	5031–5325
Poz-68,006	8.55	Bulk	4060 ± 50	4421–4653
Poz-72,529	8.85	Bulk	4320 ± 35	4837–4969
Poz-72,527	9.65	Bulk	4405 ± 35	4861–5058
Poz-64,892	10.2	Bulk	4410 ± 40	4862–5067
Poz-72,526	11.75	Bulk	3345 ± 35	3479–3644
Poz-63,659	12.13	Bulk	4710 ± 30	5323–5417
Poz-63,660	12.5	Terrestrial organic matter	5470 ± 30	6209–6310
Poz-63,661	13.05	Terrestrial organic matter	5160 ± 30	5890–5990
Poz-72,531	14.05	Bulk	5560 ± 40	6288–6410
Poz-63,662	15.18	Terrestrial organic matter	6225 ± 30	7016–7249
Poz-63,663	15.23	Terrestrial organic matter	6140 ± 35	6945–7160
Poz-63,587	16.04	Terrestrial organic matter	6630 ± 40	7456–7575
Poz-63,854	16.1	Terrestrial organic matter	6660 ± 35	7473–7588
Poz-63,588	16.42	Bulk	6750 ± 50	7560–7680
Poz-63,589	16.48	Bulk	6850 ± 40	7608–7763
Poz-63,590	17.45	Terrestrial organic matter	7360 ± 50	8038–8317
Poz-63,591	17.63	Terrestrial organic matter	7480 ± 40	8199–8377
Poz-72,525	18.25	Bulk	7910 ± 40	8599–8799
Poz-72,530	19.75	Bulk	15,320 ± 80	18,393–18,768
Poz-72,538	19.95	Bulk	12,750 ± 80	14,860–15,500
Poz-72,535	20.85	Bulk	11,910 ± 80	13,554–13,983

3.2. Grain size analysis

Grain size analysis was conducted using a Beckman Coulter Laser Diffraction Particle Size Analyser (Model: LS13320), with a measurement range of 0.04–2000 μm, at the State Key Laboratory of Estuarine and Coastal Research, East China Normal University (SKLEC, ECNU). Samples were dried at 40 °C for 24 h, then 10% HCl was added to eliminate carbonates, 10% H_2O_2 was added to remove organic matter, and finally $Na(PO_3)_6$ was added to disperse the samples before testing.

3.3. TOC and carbonates measurements

TOC was determined by using the wet oxidation method with $K_2Cr_2O_7$ as an oxidant and titration was performed using ferrous ammonium sulfate (Lu, 2000). The carbonate contents (in the form of $CO_3^{2-} + HCO_3^{-}$) were calculated by the acid-alkali neutralization titration method (Bao, 2000). The measurements were conducted in SKLEC, ECNU.

3.4. Magnetic analysis

The sediment magnetic susceptibilities were measured using a Bartington Instruments MS2 magnetic susceptibility metre at low (0.47 kHz) frequency (χ_{lf}). An anhysteretic remnant magnetization (ARM) was imparted in a 0.04 mT direct current (DC) bias field that was superimposed on a peak alternating field (AF) of 100 mT using a DTECH 2000 AF demagnetizer and was measured using a Molspin magnetometer. ARM is expressed as anhysteretic susceptibility (χ_{ARM}) by normalizing ARM by the applied DC field. Isothermal remnant magnetization (IRM) measurements were made using a forward field of 1 T followed by application of −300 mT backfields which were imparted using an MMPM10 pulse magnetizer. The IRM imparted with a 1 T induction is referred to as the 'saturation' IRM (SIRM). S_{-300mT} was calculated as $S_{-300mT} = 100 \times (SIRM\text{-}IRM_{-300mT})/(2 \times SIRM)$ (Bloemendal and Liu, 2005). The tests were conducted in the environmental magnetism lab of SKLEC, ECNU (Jiang et al., 2016).

3.5. Element measurements and multivariate statistical analysis

Samples were measured by weighing 1.0 g of dried sediment in porcelain crucibles. To avoid contamination, crucibles were first cleaned with concentrated HCl and heated at 1100 °C for 30 min. Approximately 4.0 g of lithium tetraborate ($Li_2B_4O_7$), 0.4 g of lithium carbonate powder (Li_2CO_3), and 0.1 g of ammonium nitrate (NH_4NO_3) were added to the samples. After thorough stirring, the samples were heated in platinum containers to 1200 °C for 8 min. The sediment elemental tests were done using an Axios Advanced XRF Spectrometer (Model, PW4400) at the Institute of Earth Environment, Chinese Academy of Sciences in Xi'an (IEECAS). Calibration was done with 26 certified reference materials from China (fifteen soil samples (GSS 1–7 and 9–16) and 11 stream sediment samples (GSD 1–11)). Analytical uncertainties, as verified by parallel analysis of two standards (GSS 8, GSD 12), were better than 2%. The major (Al_2O_3, SiO_2, TFe_2O_3, CaO, MgO, K_2O, Na_2O) and trace element (Ti, Cr, Ni, Mn, Zn, Rb and Sr) results in oxide form were in percentages (%) and in parts per million (ppm). Elements normalized to Al were calculated as Al is the most insoluble (under both oxic and anoxic conditions) and common terrestrially derived element (exclusively derived from detrital aluminosilicate sources). The relationship between Al_2O_3 and major oxides can be used to deduce the source of lake sediments (Murray et al., 1992; Brown et al., 2000).

For multivariate statistical analysis, principal component analysis (PCA) was applied to the 14 measured elements and the mean grain size data to assess their interrelationship using the SPSS 23 software package. In the present study, Bartlett's sphericity tests and Kaiser-Meyer-Olkin (KMO) were used to identify the adequacy of the PCA results.

4. Results

4.1. Lithology of FA-1 core

Various sediment sections were recognized in core FA-1 according to changes in sediment grain size, structure, colour, bio-detritus and the distribution of evaporates (Fig. 2). From the core bottom upwards, it consists of: yellowish and brownish fine to medium sand at a core depth of 21.25–20.20 m; greyish clayey silt with bio-detritus at 20.20–18.00 m; dark greyish clayey silt with thin laminae at 18.00–13.00 m; greyish clay silt with laminated diatomite and mollusc shells at 13.00–11.70 m; greyish clayey silt with diatom and ferruginous laminae at 11.70–10.80 m; greyish clayey silt interbedded with a few thin gypsum laminae at 10.80–7.50 m; greyish silty clay with gypsum at 7.50–4.30 m and plants residues was seen at 5.40–4.30 m; greyish silt clay with ferruginous oxides at 4.30–1.90 m (Fig. 2).

For the grain size of the sediment, bi-modal and unimodal grain size distribution curves (main modes at 470–820 μm) occurred at the bottom of the core. Towards the top of the core, the grain size composition mainly showed unimodal curves with main modes between ~20–40 μm (~20.20–18.00 m) and ~10–20 μm (18.00–13.00 m). At depths of 13.00–10.80 m, unimodal grain size distribution curves dominated with varied modes between ~2–200 μm. Unimodal grain size distribution curves with modes between ~10–50 μm were recorded for most samples at depths of 10.80–7.50 m. Sediment between 7.50 and 5.40 m had unimodal distribution curves with a few bi-modal ones, with modes ranging between ~10–100 μm. For the uppermost part of the core, unimodal distribution curves prevailed with modes between ~6–50 μm (Fig. 2).

4.2. Age-depth model

Bacon software implemented with the statistical software package R was used to show the age-depth model of core FA-1 (Fig. 3). It indicated that the base of the silty sediment overlying the sandy deposits was estimated to be *ca.* 9.7 cal ka BP at a depth of 20.20 m, yielding an average sediment accumulation rate of ~1.88 mm/a throughout the Holocene. The sedimentation rate was approximately 1.84 mm/a prior to *ca.* 5.5 cal ka BP and approximately 1.33 mm/a in the last *ca.* 4.0 ka. Rapid sedimentation (~3.60 mm/a) was observed in the middle section of the core *ca.* 5.5–4.0 ka BP.

4.3. Organic matter and carbonates

TOC of core FA-1 showed obvious variations from the core bottom upwards (Fig. 4). It was low (< 1%) prior to *ca.* 9.7 cal ka BP (below the core depth of 20.2 m), then rose to > 3% during *ca.* 9.7–5.0 cal ka BP (at a depth of 20.2–13.1 m). After that it declined gradually but with a small peak *ca.* 2.7–2.3 cal ka BP (at a depth of 5.6–4.2 m). The carbonates in the sediment exhibited highs *ca.* 9.7–8.4 cal ka BP (below the depth of 18.0 m) and in the last *ca.* 4.5 ka (above the core depth of 7.9 m). Relative low values of carbonates occurred between *ca.* 8.4 and 4.5 cal ka BP (at a depth of 18.0–7.9 m).

4.4. Sediment magnetism features

Briefly, sediment magnetism parameters enable the core to be divided into magnetically similar zones (Fig. 4). The magnetic properties of χ, SIRM, and χ_{ARM} showed similar upward increasing trends. They exhibited extreme low values prior to *ca.* 9.7 cal ka BP. At *ca.* 9.7–8.4 cal ka BP, χ, χ_{ARM}/SIRM, and S-ratios increased while other proxies remained low. Since *ca.* 8.4 cal ka BP, the magnetic proxies showed slight increases until *ca.* 5.0 cal ka BP (Fig. 4), then most of them increased drastically, especially noticeable are the highs of χ, SIRM, χ_{ARM} and χ_{ARM}/SIRM at *ca.*5.0–2.7 cal ka BP. A sharp decrease in χ, SIRM, χ_{ARM}, and χ_{ARM}/SIRM were marked at *ca.*2.7 cal ka BP, but the concentration of related proxies (χ, SIRM) recovered and increased rapidly afterwards. In general, S_{-300mT} and SIRM/χ exhibited steadily increasing trends from the bottom upwards, except for two higher values *ca.* 9.7 and 8.3 cal ka BP.

4.5. Elemental data

The sediment elemental data showed several major changes as follows: evident highs of SiO_2 and CaO with lows of Al_2O_3, TFe_2O_3 (total of FeO and Fe_2O_3), MgO, Na_2O, TiO_2 and Sr (Fig. 5 A) were seen prior to the Holocene. It is followed by highs of MgO, CaO, Sr and lows of SiO_2 during *ca.* 9.7–8.4 cal ka BP. Then there were minor changes in all the elements during *ca.* 8.4–5.0 cal ka BP. SiO_2 abundance showed a sharp decline while TiO_2 abundance increased after *ca.* 5.0 cal ka BP.

For element ratios, highs in Ti/Al and Si/Al occurred prior to *ca.* 9.7 cal ka BP (Fig. 5B). In contrast, Ti/Al increased as Si/Al remained low after *ca.* 5.0 cal ka BP. Mg/Al and Ca/Al showed highs during *ca.* 9.7–8.4 cal ka BP while Ti/Al and Si/Al were lower. Ratios of all elements remained stable during *ca.* 8.4–5.0 cal ka BP, and noticeable increases in Ti/Al, Na/Al, Mg/Al, K/Al occurred after *ca.* 5.0 cal ka BP (Fig. 5B).

The KMO and Bartlett's Test revealed acceptable suitability of the PCA for the elemental data obtained from FA-1 (Table 2). Three main

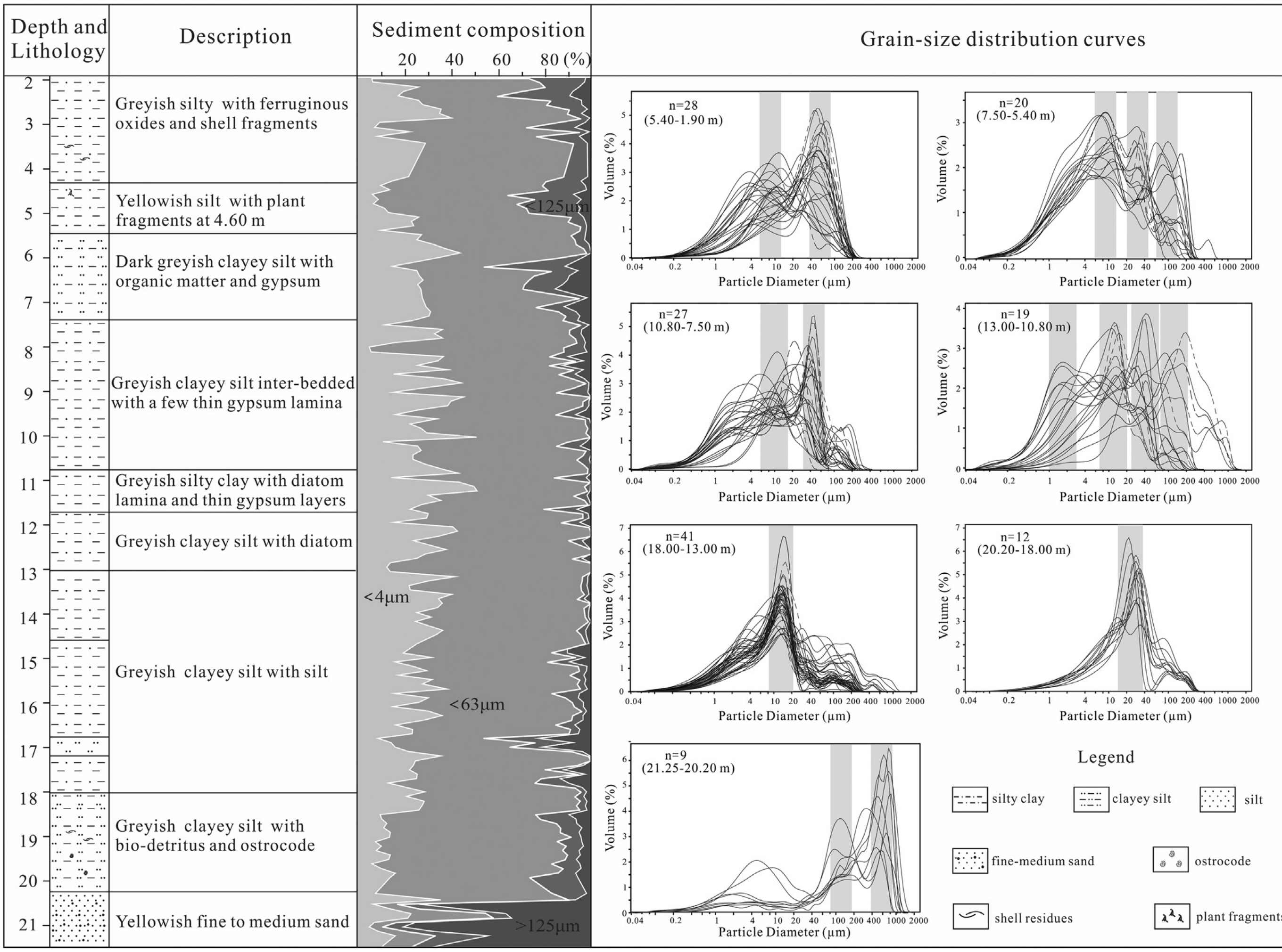

Fig. 2. Lithology, sediment composition and grain size distribution curves of FA-1 core. The grey columns show the main modes of the grain size distribution curves.

components were derived from the variables and have eigenvalues > 1.6, accounting for 80% of the total variance (Table 3). The first component, with 48% of the total variance, includes positive loadings for Ti, Cr, Ni, Zn, Rb, Al_2O_3, Fe_2O_3, MgO, Na_2O, and K_2O and negative loadings for Sr and CaO. The second component represents 21% of the total variance and has positive loadings of Sr, MgO, CaO, and Na_2O and negative loading of SiO_2. The third component occupies 11% of the total variance with negative loadings of redox-sensitive elements Mn and Fe_2O_3 (Tables 3 and 4).

5. Discussion

5.1. Signature of the magnetic properties and sediment geochemistry in Faiyum Basin

Sediment magnetic properties are usually controlled by the provenance, grain size and post-depositional processes, which are considered linked with regional climate, environmental change and human activities (Thompson and Oldfield, 1986; Oldfield, 1999; Liu et al., 2012; Roberts, 2015). Significant correlations between χ and SIRM ($r^2 = 0.9872$) and no rules of χ with a mean grain size suggested that ferrimagnetic minerals dominated the sediment magnetism with minor effects from grain size variations (Fig. 6). Changes in ratios of χ_{ARM}/SIRM and SIRM/χ ($< 20 \times 10^3$ Am^{-1}) also excluded the evident occurrence of diagenetic and authigenic greigite in the sediment (Oldfield, 1999; Foster et al., 2008). As indicated by previous studies in Faiyum Basin, the contribution of secondary and soil-derived ferrimagnets to the sediment magnetism were also minor (Foster et al., 2008; Jiang et al., 2016). Thus, the variations in sediment magnetic properties in core FA-1 mainly reflected changes in sediment provenance since the last *ca.* 9.7 ka BP.

The elemental features of the lake sediment are fundamentally determined by the sediment provenance, sedimentary environment and the chemical weathering intensity of the lake catchment. As the Faiyum Basin is located in a region of North Africa that was arid during the entire Holocene (Kuper and Kröpelin, 2006), the extremely low rainfall would make local chemical weathering intensity particularly weak. Thus, the key factors affecting the elemental characteristics of the sediment are the changes in sediment provenance and the depositional setting.

High positive loadings of Ti, Cr, Ni, Zn, Rb, Al_2O_3, Fe_2O_3, MgO, Na_2O and K_2O in component 1 from the PCA implied that the vertical distribution of these elements could be controlled by the same source, likely the detrital provenance derived from the Nile flood water. Component 2 includes high loadings of Sr, MgO and CaO, which are mobile elements derived primarily from carbonates of authigenic calcite and aragonite in the lake. Component 3 is marked by high loadings of Mn and Fe_2O_3 which are sensitive to the oxidation-reduction environment in the lake. Additionally, poor correlations of mean grain size with all the elements are exhibited (Fig. 5) (Table 4), suggesting its minor effects on the elemental features of the sediments.

The Nile drains markedly different geologic terrains and climate zones, thus the elemental features of the riverine materials could contain the imprints of diverse basement rocks of the Nile basin. The White

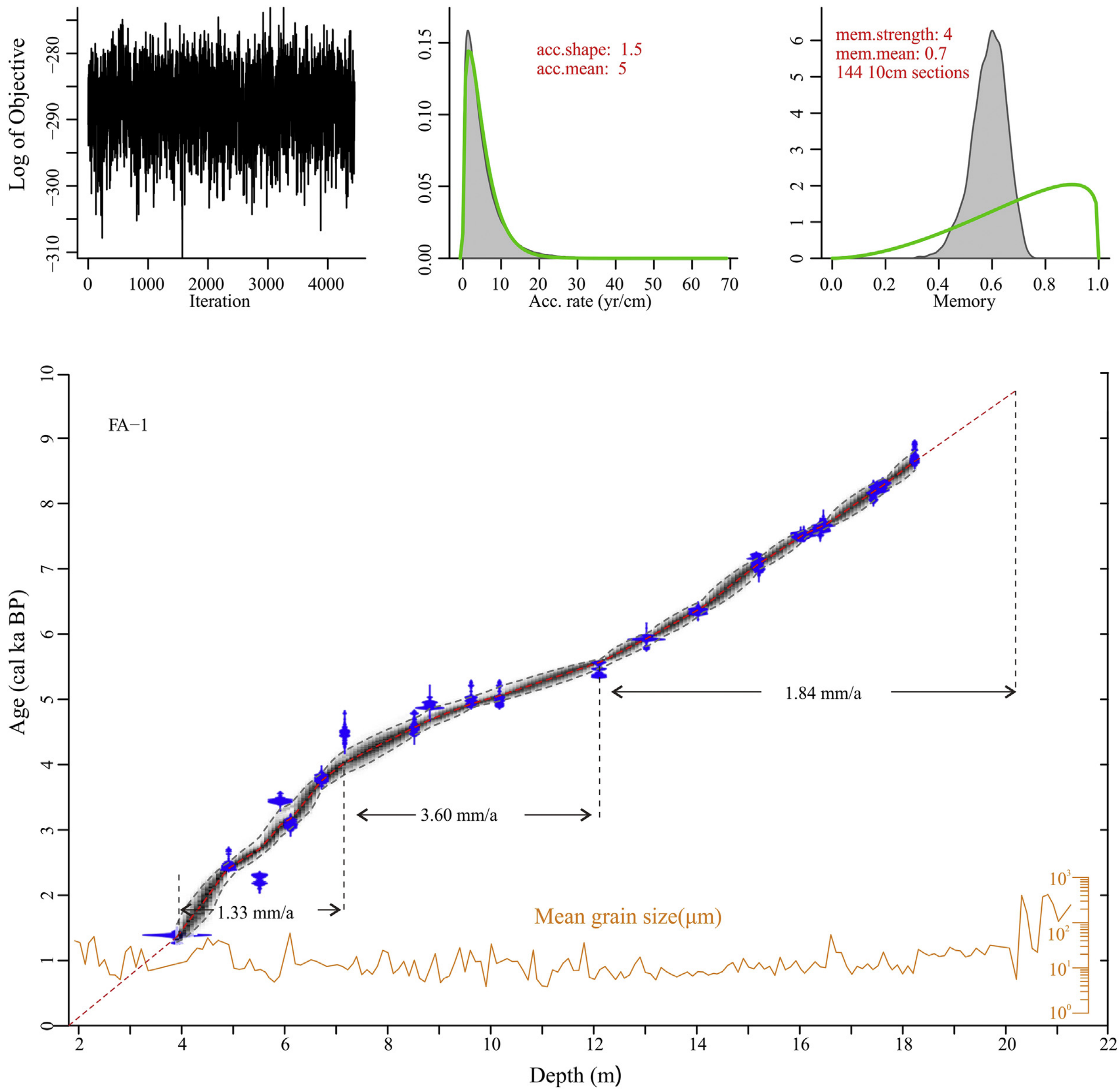

Fig. 3. Age-depth model of FA-1 core. Dashed lines indicate the 95% confidence range and the solid red line shows the medium ages for each depth. The mean grain size is illustrated to help understand the transitions of sedimentation rate. (For interpretation of the references to colour in this figure legend, the reader is referred to the web version of this article.)

Nile drains predominantly crystalline basement rocks, whereas the Blue Nile and the Atbara flow off the Ethiopian Highlands, which consists of Tertiary volcanic rocks (Krom et al., 2002; Garzanti et al., 2015). The chemical composition of the White Nile sediment from northern Uganda to South Sudan is similar to the upper continental crust (UCC) but is enriched in Si and depleted in mobile alkali and alkaline earth metals. The Blue Nile and Atbara sediments have higher Ti, revealing their basaltic origin from the Ethiopian Traps. Along the lower course of the Nile, feldspathic-quartzose of fine to medium-grained aeolian sand would add relatively high abundances of K and Na (Garzanti et al., 2015). The surrounding desert contributes quartz-rich sandy deposits to the Faiyum Basin, which normally has high Si/Al ratios due to the virtual absence of aluminium from clay-bearing silicates (Davies et al., 2015).

Thus, different elemental features of Faiyum sediment combined with changes in the sediment magnetic properties could be used to trace the contrasting contributions of their major sediment sources and sedimentary environment as mentioned above. Relatively high values of Ti and the Ti/Al ratio with high sediment magnetism suggests an increased contribution of riverine detrital material from flood basalts of the Ethiopian Highlands carried by Blue Nile and the Atbara discharge. The highs in Si and the Si/Al ratio imply a major contribution from the surrounding deserts. Since the basement geology of the Faiyum Basin is mainly Eocene limestone (Wendorf and Schild, 1976; Said, 1993), the higher values of Ca and Mg in the sediment reflects the dissolution of basal calcium and magnesium carbonate by water leaching (Fig. 5A, B).

5.2. The sediment provenance of the Faiyum Basin during the Holocene

Elemental features combined with changes in sediment grain size and magnetic properties of core FA-1 exhibited several major shifts in sediment provenance during the Holocene.

Prior to *ca.* 9.7 cal ka BP, the brownish coarser sediment with high Si/Al ratios, and low χ and S_{-300mT} indicated a major contribution of quartz-rich material with few ferrimagnetic minerals. The unimodal grain size distribution curves for most of the samples are characteristic of desert dune sand in this region, and the quartz from the sediments is similar in nature to local sand dunes and those from the Sahara Desert

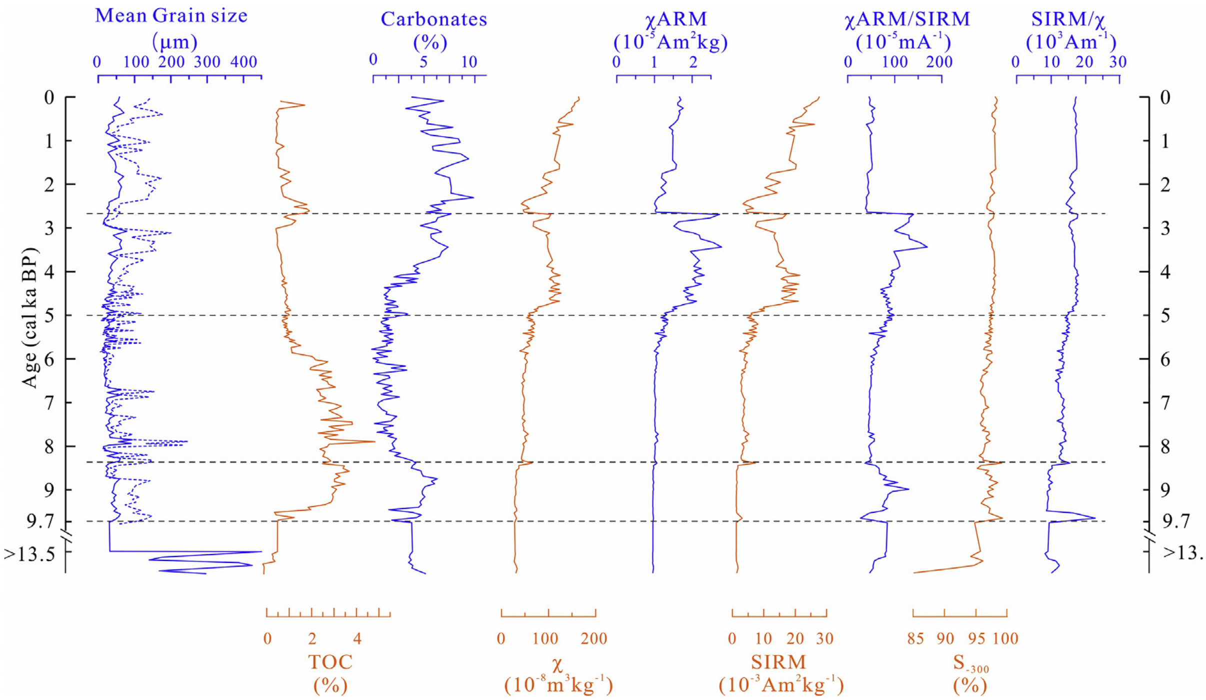

Fig. 4. Magnetic properties of the core sediment, also included are the mean grain size, content of total organic carbon (TOC) and the carbonates(in form of CaCO3). The grey line in mean grain size column shows 3 times magnification. Dash lines in grey indicate transitions in the magnetic proxies at *ca.*9.7, 8.4, 5.0, and 2.7 cal ka BP.

(Zhao et al., 2017). This together with the lowest amount of organic matter in the sediment demonstrated that the bottom section of core FA-1 was mainly of aeolian origin from local sand-drifts (Figs. 2, 4 and 5).

The sediment grain size showed different distribution patterns before and after *ca.* 9.7 cal ka BP (core depth 20.20 m), hinting at a brief change in the sedimentation process since then (Fig. 2). The sediment became finer during *ca.* 9.7–5.0 cal ka BP, meanwhile, most of the elements and their ratios to Al exhibited minor variations with only slight increases in sediment magnetic parameters (Figs. 4 and 5). This would imply a stable input of detrital material from Nile discharge into the Faiyum Basin, which is significantly different from the aeolian origin of the surrounding sand dunes. The initial high values of Mg, Ca, and Sr during *ca.* 9.7–8.4 cal ka BP may reflect leaching processes when the basement carbonate is dissolved by the Nile water; this would also support the high values of carbonates (Figs. 4 and 5). Thus, the Nile became a major contributor to water and sediment entering Faiyum Basin since 9.7 cal ka BP.

After *ca.* 5.0 cal ka BP, varied modes of the sediment grain size distribution curves revealed changing hydrodynamics in the lake, possibly related to Nile discharge fluctuations (Fig. 2). Increasing Ti and Ti/Al ratios, with notable increases in some of the magnetic proxies (χ, SIRM, χ_{ARM}, and χ_{ARM}/SIRM), occurred after *ca.* 5.0 cal ka BP. This suggests increasing sediment discharge from the Blue Nile and the Atbara, which carried abundant volcanic sediment from the Ethiopian Highlands, rich in Ti and magnetic minerals. In contrast, less Ti and weaker magnetism were linked to the crystalline basement rocks in the White Nile drainage area (Krom et al., 2002). The Na/Al and K/Al ratios also suggests an increasing contribution of aeolian sand which is rich in feldspathic-quartzose from the lower course of the Nile.

The past 2.7 cal ka BP recorded not only higher Ti, Ti/Al ratio, χ, SIRM, and HIRM but a sharp fall in $\chi_{ARM,}$ and χ_{ARM} /SIRM, indicating the prevalence of coarser magnetic grains in the sediment. This agreed with the grain size distribution curves which exhibited a coarsening trend (Fig. 2). However, minor changes in S_{-300mT}, SIRM/χ and Si/Al ratio suggests there were minor alternations in sediment provenance. This probably reflects increasing hydrological modifications and regulations by humans in the Faiyum Basin during the last two millennia as suggested by previous studies (Hassan et al., 2012).

5.3. The Holocene Basin-Nile connection and the climate of the Nile

Sediment provenance changes in core FA-1 show a close hydrological linkage between the Faiyum Basin and the Nile. This is helpful for better understanding the Nile discharge and climate changes in the Nile catchment since the Holocene.

Prior to the Holocene, the sediment in core FA-1 was mainly of aeolian origin, indicating a dry basin. Similarly, aeolian sand deposits were recorded by other neighbouring sediment cores F1–08, QARU9 and Tersa at depths of ~20 m, with an age of ~10.0 cal ka BP (Flower et al., 2012; Hamdan et al., 2016). These core records confirmed that there was no Nile discharge into the basin before *ca.* 9.7 cal ka BP, and thus no hydrological connection between the Faiyum Basin and the Nile. The Faiyum Basin sediment was predominantly sourced from the Nile from *ca.* 9.7–5.0 cal ka BP, indicating a persistent hydrological connection to the Nile. This coincided with a freshwater lake environment from *ca.* 9.7 cal ka BP as freshwater ostracods and diatoms appeared in the sediment, and productivity was higher as implied high TOC (Figs. 2 and 3) (Marks et al., 2018). A deep freshwater setting recorded by freshwater diatom species of a neighbouring core, Tersa, dated as early as 9.9–8.5 ka BP (Hamdan et al., 2016), and a high lake level stage reconstructed to *ca.* 9.8–5.0 cal ka BP also supports large water and material contributions of the Nile (Fig. 7a) (Hassan, 1986; Hassan et al., 2012).

After *ca.* 5.0 cal ka BP, the sediment contribution from the volcanic Ethiopian Highlands to the Faiyum Basin became dominant (Figs. 5B and 7b-e). Previous records of Sr^{86}/Sr^{87} and Ti/Al ratios from deltaic sediments also revealed an increasing riverine sediment discharge from the Blue Nile and the Atbara (Krom et al., 2002) (Fig. 7f), and a declining contribution from the White Nile (Blanchet et al., 2015) (Fig. 7g). Since the Blue Nile and the Atbara carried massive sediment fluxes during flood seasons when the ASM prevailed over the Ethiopian

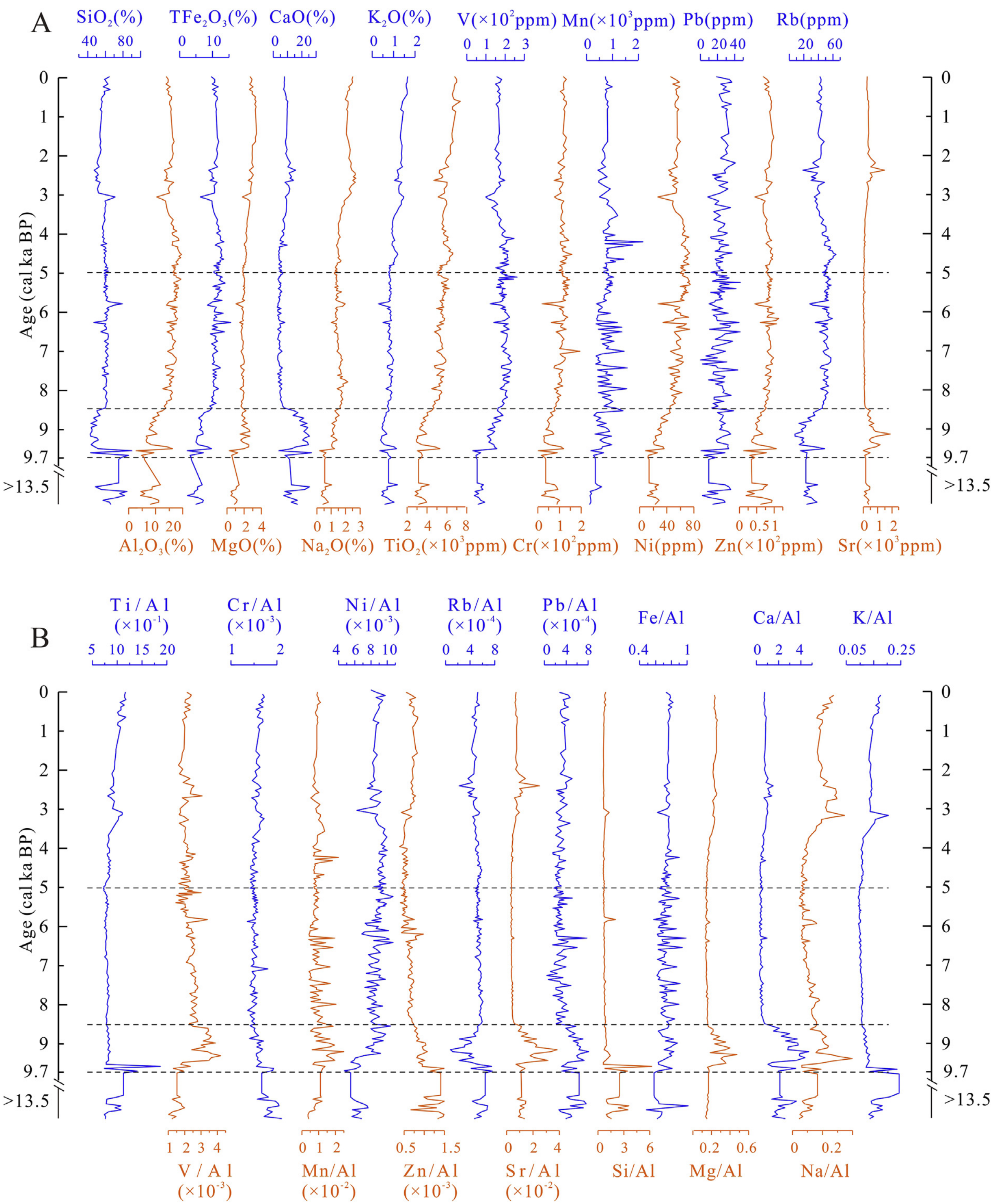

Fig. 5. (A) Contents of major and trace elements of the core sediment with changes of sediment mean grain size; (B) ratios of different elements normalized to Al. Dash lines in grey classify the vertical variations in the geochemical features.

Table 2
The results of KMO and Bartlett's Test

Kaiser-Meyer-Olkin Measure of Sampling Adequacy		0.801
Bartlett's Test of Sphericity	Approx. Chi-Square	3943.794
	df	105
	Sig.	0.000

Highlands (Garzanti et al., 2015), such a change in the sediment provenance pattern marks the weakening of the Nile-Basin connection with notable seasonality since *ca.* 5.0 cal ka BP. Although the connection of the Faiyum Basin to the Nile strengthened *ca.* 2.7–2.3 cal ka BP, it was likely associated with a man-made canal linking the Nile to the Faiyum Basin (Ball, 1939). In the last 2000 years, the basin was increasingly influenced by man-made canals, implying a further weakening of the natural hydrological connection with the Nile (Fig. 7b-e).

The hydrological connection between the Faiyum Basin and the Nile

Table 3
The total variance explained for the component.

component	Initial Eigenvalues			Extraction Sums of Squared Loadings			Rotation Sums of Squared Loadings		
	Total	% of Variance	Cumulative %	Total	% of Variance	Cumulative %	Total	% of Variance	Cumulative %
1	7.201	48.005	48.005	7.201	48.005	48.005	5.458	36.386	36.386
2	3.149	20.993	68.998	3.149	20.993	68.998	4.209	28.061	64.447
3	1.657	11.050	80.048	1.657	11.050	80.048	2.340	15.600	80.048
4	0.950	6.331	86.379						
5	0.835	5.567	91.946						
6	0.379	2.526	94.472						
7	0.241	1.609	96.081						
8	0.193	1.287	97.368						
9	0.140	0.930	98.298						
10	0.089	0.590	98.888						
11	0.058	0.390	99.278						
12	0.053	0.354	99.632						
13	0.023	0.150	99.782						
14	0.021	0.139	99.921						
15	0.012	0.079	100.000						

Extraction Method: Principal Component Analysis.

Table 4
The component matrix and the rotated component matrix.

	Component			Component		
	1	2	3	1	2	3
Ti	0.918	0.253	0.189	0.645	0.721	0.086
Cr	0.880	0.046	0.113	0.719	0.511	0.107
Mn	0.104	0.008	−0.863	0.010	−0.202	0.846
Ni	0.907	−0.109	−0.066	0.810	0.345	0.251
Zn	0.768	0.036	0.068	0.626	0.433	0.121
Rb	0.889	−0.386	0.014	0.953	0.134	0.112
Sr	−0.512	0.759	−0.010	−0.842	0.357	0.050
SiO_2	0.067	−0.771	0.437	0.512	−0.462	−0.561
Al_2O_3	0.957	−0.084	−0.012	0.843	0.406	0.216
Fe_2O_3	0.757	−0.028	−0.582	0.598	0.180	0.723
MgO	0.465	0.831	0.073	−0.059	0.929	0.213
CaO	−0.764	0.563	−0.074	−0.950	0.054	0.011
Na_2O	0.485	0.614	0.206	0.088	0.803	0.046
K_2O	0.568	0.553	0.383	0.205	0.848	−0.116
Mean Grain Size	−0.508	−0.226	0.353	−0.271	−0.331	−0.500

Extraction Method: Principal Component Analysis; Rotation Method: Varimax with Kaiser Normalization.

further reflected climatic variations across the south to north of East Africa and local hydrological modifications by ancient humans. The Nile was dry with less rainfall prior to *ca.* 9.7 cal ka BP, as it prevented Nile discharge from supplying the Faiyum Basin. A northerly shift in the ITCZ in response to solar insolation since the early Holocene led to an enhanced ASM and a green Sahara (Kutzbach, 1981; Kuper and Kröpelin, 2006; Marriner et al., 2012) (Fig. 7 h-i). Durative Nile discharge into the Faiyum Basin during *ca.* 9.7–5.0 cal ka BP also revealed strong runoff and frequent overbank floods in the lower reaches of the Nile. It clearly indicated the humid period of the Nile basin in the Holocene. The weakening of the hydrological connection with the Nile began *ca.* 5.0 cal ka BP, implying a decreasing discharge of the main Nile. This reflected the decaying ASM and the southward shift of the ITCZ after the middle Holocene. As the ASM rain belt retreated from the northern Sahara (Johnson et al., 2002), the climate became drier over the lower reaches of the Nile Basin (deMenocal et al., 2000) (Fig. 7j). Although the Faiyum Basin was still fed by Nile materials after *ca.* 5.0 cal ka BP, a further drying of the Nile Basin is suggested due to the digging of Bahr Yosef canal connecting the Faiyum Basin with the Nile for irrigation and daily water needs during the reign of Amenemhat I (1980–1970 BCE) (Butzer, 1976), and increasing hydrological modifications by humans in the basin in the last 2000 years.

6. Conclusions

The combined geochemistry, grain size and magnetic properties of the sediment in Faiyum Basin can serve as reliable indicators of changes in sediment provenance in association with climate-induced Nile discharge. Thus, this study provides some insights into the environment of the lower Nile region in response to the climate of the Nile Basin since

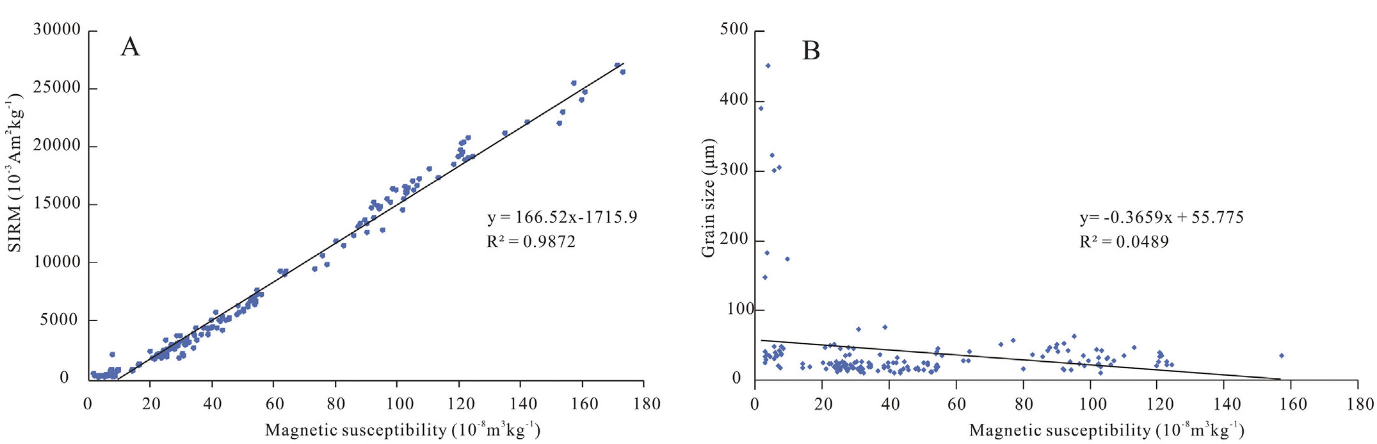

Fig. 6. (A) correlation of sediment magnetic susceptibility (χ) with saturation isothermal remanence (SIRM); and (B) sediment magnetic susceptibility (χ) with mean grain size.

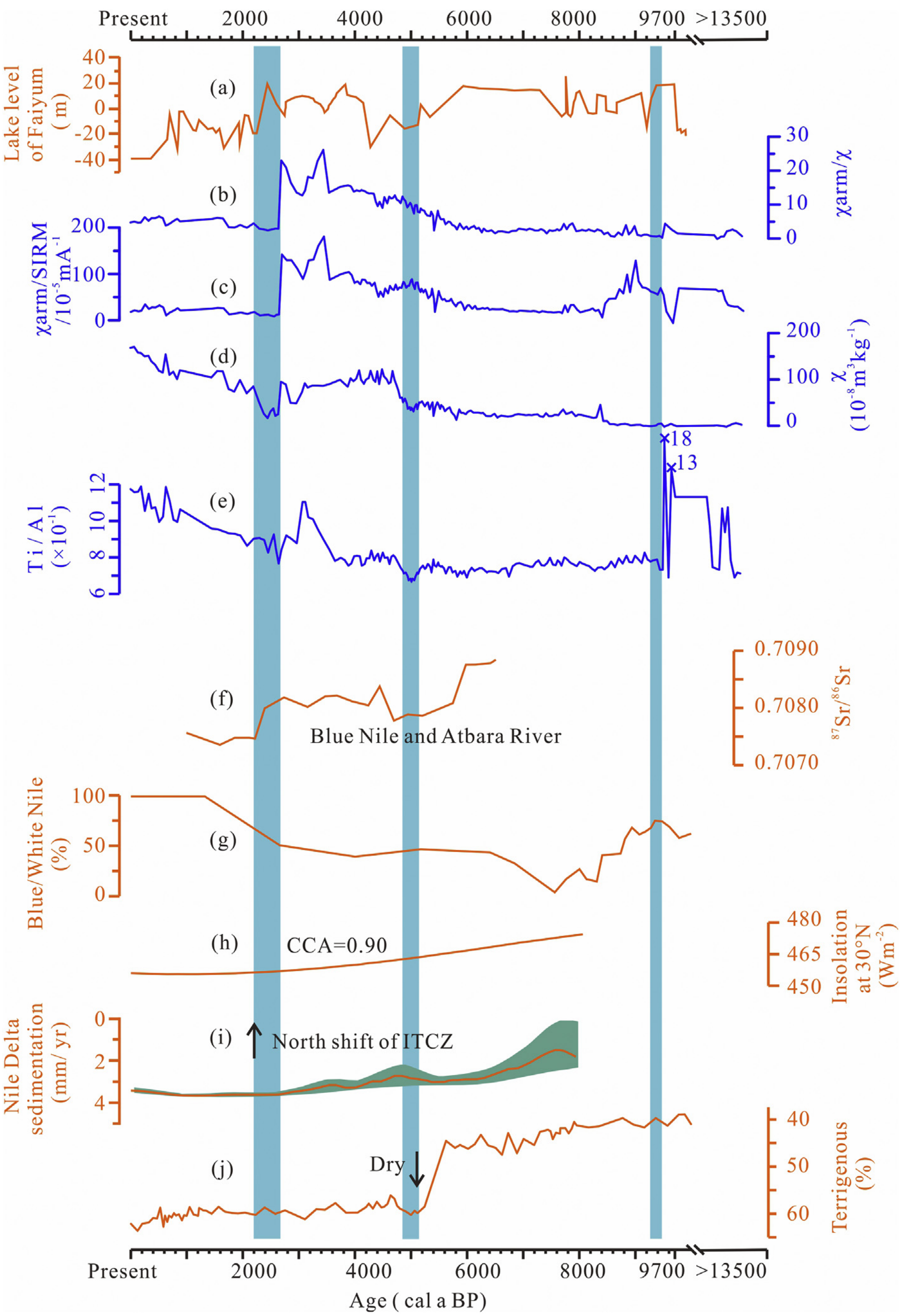

Fig. 7. Variations of sediment sources of the Faiyum Basin in the Holocene *versus* other proxies. (a) Faiyum lake level (Modified after Hassan, 1986; Hassan et al., 2012); (b,c) indicative of relative input from the Blue Nile and Atbara River, but also including information of human interferences during the past 2000 years; (d,e) indicative of relative input from the Blue Nile and Atbara River; (f) $^{87}Sr/^{86}Sr$ from core S-21 in the Nile delta showing relative contribution from the Blue and the White Nile (Stanley and Goodfriend, 1997; Krom et al., 2002; Woodward et al., 2007); (g) Blue/White Nile contribution to the main Nile (Blanchet et al., 2015); (h) Insolation of 30°N (Berger, 1978); (i) Nile delta sedimentation rate (Marriner et al., 2012); (j) Variations in terrigenous (aeolian) sediment import off Cap Blanc (Mauritania) recording past changes in aridity over the Saharan region (deMenocal et al., 2000). (For interpretation of the references to colour in this figure legend, the reader is referred to the web version of this article.)

the Holocene. Sandy deposits of aeolian origin prior to *ca.* 9.7 cal ka BP reflected a hyper-dry basin setting. There would be no connection between the basin and the Nile by overbank floods, as the Nile was dry. The Faiyum Basin was fed primarily by Nile discharge after *ca.* 9.7 cal ka BP, revealing a durative hydrological connection to the Nile by frequent overbank floods. This would mark a humid Nile since then. A drying Nile occurred after *ca.* 5.0 cal ka BP, as materials from the Ethiopian Highlands carried by the Blue Nile and the Atbara became dominant in the Faiyum Basin. The humid Nile period during *ca.* 9.7–5.0 cal ka BP reflects increasing monsoon rainfall in both the headwater and the northern regions of the Nile basin driven by the northward migration of the ITCZ in the Northern Hemisphere. A drying Nile after *ca.* 5.0 cal ka BP reflects declining monsoon rainfall caused by the southward retreat of the ITCZ. This may account for the failure of the old Kingdom approximately 4.2 cal ka BP in the Egypt. The present study also provided geological evidence of intensified human activities in the Faiyum Basin since 4.0 cal ka BP, especially in the last 2.7 cal ka BP. The hydrological regulations made by human, such as channel digging connecting the Nile, enables the survival of Lake Qarun in the Faiyum Basin under a hyper-arid climate setting.

Acknowledgements

The work is financially supported by the National Natural Science Foundation of China (Grant Nos. 41671199, 41501005 and 41620104004), and drilling and radiocarbon dating were supported by the National Science Centre in Poland (decision no. DEC-2012/05/B/ST10/00558). The authors thank the synonymous reviewers for their constructive comments and suggestions. We also thank Dr. Brian Finlayson for his great effort in smoothing the language of this manuscript.

References

Baioumy, H.M., Kayanne, H., Tada, R., 2010. Reconstruction of Lake-level and climate changes in Lake Qarun, Egypt, during the last 7000 years. J. Great Lakes Res. 36, 318–327.
Baioumy, H., Kayanne, H., Tada, R., 2011. Record of Holocene aridification (6000–7000BP) in Egypt (NE Africa): Authigenic carbonate minerals from laminated sediments in Lake Qarun. Quat. Int. 245, 170–177.
Ball, J., 1939. Contributions to the Geography of Egypt.
Bao, S.D., 2000. Soil and Agricultural Chemistry Analysis. China Agriculture Press, Beijing, pp. 495 (in Chinese).
Beadnell, H.J.L., 1905. Topography and geology of the Faiyum Province of Egypt. Survey Department of Egypt, Cairo, pp. 101.
Berger, A., 1978. Long-term variations of daily insolation and Quaternary climatic changes. J. Atmos. Sci. 35, 2362–2367.
Bernhardt, C.E., Horton, B.P., Stanley, J.D., 2012. Nile delta vegetation response to holocene climate variability. Geology 40, 615–618.
Blaauw, M., Christen, J.A., 2011. Flexible paleoclimate age-depth models using an autoregressive gamma process. Bayesian Anal. 6, 457–474.
Blanchet, C.L., Contoux, C., Leduc, G., 2015. Runoff and precipitation dynamics in the Blue and White Nile catchments during the mid-Holocene: a data-model comparison. Quat. Sci. Rev. 130, 222–230.
Bloemendal, J., Liu, X., 2005. Rock magnetism and geochemistry of two Plio–Pleistocene Chinese loess–palaeosol sequences–implications for quantitative palaeoprecipitation reconstruction. Palaeogeogr. Palaeoclimatol. Palaeoecol. 226, 149–166.
Brown, E.T., Le Callonnec, L., German, C.R., 2000. Geochemical cycling of redox-sensitive metals in sediments from Lake Malawi: a diagnostic paleotracer for episodic changes in mixing depth. Geochim. Cosmochim. Acta 64, 3515–3523.
Bubenzer, O., Riemer, H., 2007. Holocene climatic change and human settlement between the Central Sahara and the Nile Valley: archaeological and geomorphological results. Geoarchaeology 22, 607–620.
Butzer, K.W., 1976. Early Hydraulic Civilization in Egypt: A Study in Cultural Ecology. Prehistoric Archeology and Ecology (USA).
Castañeda, I.S., Caley, T., Dupont, L., Kim, J.-H., Malaizé, B., Schouten, S., 2016. Middle to late Pleistocene vegetation and climate change in subtropical southern East Africa. Earth Planet. Sci. Lett. 450, 306–316.
Davies, S.J., Lamb, H.F., Roberts, S.J., 2015. Micro-XRF core scanning in palaeolimnology: recent developments. In: Croudace, I.W., Rothwell, R.G. (Eds.), Micro-XRF Studies of Sediment Cores: Applications of a Non-destructive Tool for the Environmental Sciences. Springer, Dordrecht, pp. 189–226.
Demenocal, P., Ortiz, J., Guilderson, T., 2000. Abrupt onset and termination of the African Humid Period: rapid climate responses to gradual insolation forcing. Quat. Sci. Rev. 19, 347–361.
El-Shabrawy, G.M., Dumont, H.J., 2009. The Fayum depression and its lakes, The Nile. Springer, pp. 95–124.
Flower, R.J., Stickley, C., Rose, N., Peglar, S., Fathi, A., Appleby, P., 2006. Environmental changes at the desert margin: an assessment of recent paleolimnological records in Lake Qarun, Middle Egypt. J. Paleolimnol. 35, 1–24.
Flower, R., Keatings, K., Hamdan, M., Hassan, F., Boyle, J., Yamada, K., Yasuda, Y., 2012. The structure and significance of early Holocene laminated lake sediments in the Faiyum Depression (Egypt) with special reference to diatoms. Diatom Research 27, 127–140.
Foster, I.D., Oldfield, F., Flower, R.J., Keatings, K., 2008. Mineral magnetic signatures in a long core from Lake Qarun, Middle Egypt. J. Paleolimnol. 40, 835–849.
Garzanti, E., Andò, S., Padoan, M., Vezzoli, G., El Kammar, A., 2015. The modern Nile sediment system: Processes and products. Quat. Sci. Rev. 130, 9–56.
Hamann, Y., Ehrmann, W., Schmiedl, G., Krüger, S., Stuut, J.B., Kuhnt, T., 2008. Sedimentation processes in the Eastern Mediterranean Sea during the late Glacial and Holocene revealed by end-member modelling of the terrigenous fraction in marine sediments. Mar. Geol. 248, 97–114.
Hamdan, M., Ibrahim, M., Shiha, M., Flower, R., Hassan, F., Eltelet, S., 2016. An exploratory early and Middle Holocene sedimentary record with palynoforms and diatoms from Faiyum lake, Egypt. Quat. Int. 410, 30–42.
Hassan, F.A., 1986. Holocene lakes and prehistoric settlements of the Western Faiyum, Egypt. J. Archaeol. Sci. 13, 483–501.
Hassan, F., Hamdan, M., Flower, R., Keatings, K., 2012. The oxygen and carbon isotopic records in Holocene freshwater mollusc shells from the faiyum paleolakes, Egypt: their paloenvironmental and paleoclimatic implications. Quat. Int. 266, 175–187.
Hoelzmann, P., Keding, B., Berke, H., Kröpelin, S., Kruse, H.-J., 2001. Environmental change and archaeology: lake evolution and human occupation in the Eastern Sahara during the Holocene. Palaeogeogr. Palaeoclimatol. Palaeoecol. 169, 193–217.
Jiang, J., Alaa, S., Lai, X.H., Zhang, W.G., Marks, L., Welc, F., Xu, L.C., Chen, J., Chen, Z.Y., Sun, Q.L., 2016. Sediment magnetism of Faiyum basin (Egypt) and its implications for the Holocene environment change. Journal of Lake Sciences 28, 1391–1403 (In Chinese).
Johnson, T.C., Brown, E.T., McManus, J., Barry, S., Barker, P., Gasse, F., 2002. A high-resolution paleoclimate record spanning the past 25,000 years in southern East Africa. Science 296, 113–132.
Krom, M.D., Stanley, J.D., Cliff, R.A., Woodward, J.C., 2002. Nile River sediment fluctuations over the past 7000 yr and their key role in sapropel development. Geology 30, 71–74.
Kuper, R., Kröpelin, S., 2006. Climate-controlled Holocene occupation in the Sahara: motor of Africa's evolution. Science 313, 803–807.
Kusky, T.M., Ramadan, T.M., Hassaan, M.M., Gabr, S., 2011. Structural and tectonic evolution of El-Faiyum depression, North Western Desert, Egypt based on analysis of Landsat ETM+, and SRTM Data. J. Earth Sci. 22, 75–100.
Kutzbach, J.E., 1981. Monsoon climate of the early Holocene: climate experiment with the earth's orbital parameters for 9000 years ago. Science 214, 59–61.
Liu, Q., Roberts, A.P., Larrasoana, J.C., Banerjee, S.K., Guyodo, Y., Tauxe, L., Oldfield, F., 2012. Environmental magnetism: principles and applications. Rev. Geophys. 50.
Lu, R., 2000. Analytic Methods of Soil and Agrochemistry. China Agriculture Press, Beijing, pp. 638 (in Chinese).
Macklin, M.G., Lewin, J., 2015. The rivers of civilization. Quat. Sci. Rev. 114, 228–244.
Marks, L., Salem, A., Welc, F., Nitychoruk, J., Chen, Z., Zalat, A., Majecka, A., Chodyka, M., Szymanek, M., Tołoczko-Pasek, A., 2016. Preliminary report on unique laminated Holocene sediments from the Qarun Lake in Egypt. Studia Quaternaria 33 (1), 35–46.
Marks, L., Salem, A., Welc, F., Nitychoruk, J., Chen, Z., Blaauw, M., Zalat, A., Majecka, A., Szymanek, M., Chodyka, M., Tołoczko-Pasek, A., Sun, Q., Zhao, X., Jiang, J., 2018. Holocene lake sediments from the Faiyum Oasis in Egypt: a record of environmental and climate change. Boreas 47 (1), 62–79.
Marriner, N., Flaux, C., Kaniewski, D., Morhange, C., Leduc, G., Moron, V., Chen, Z., Gasse, F., Empereur, J.Y., Stanley, J.D., 2012. ITCZ and ENSO-like pacing of Nile delta hydro-geomorphology during the Holocene. Quat. Sci. Rev. 45, 73–84.
Meshal, A.H., 1977. The problem of the salinity increase in Lake Qarun (Egypt) and a proposed solution. ICES J. Mar. Sci. 37, 137–143.
Murray, R.W., Jones, D.L., ten Brink, M.R.B., 1992. Diagenetic formation of bedded chert: evidence from chemistry of the chert-shale couplet. Geology 20, 271–274.
Oldfield, F., 1999. The rock magnetic identification of magnetic mineral and grain size assemblages. Environmental magnetism: a practical guide. Technical Guide 6, 98–112.
Osborne, A.H., Marino, G., Vance, D., Rohling, E., 2010. Eastern Mediterranean surface water Nd during Eemian sapropel S5: monitoring northerly (mid-latitude) versus southerly (sub-tropical) freshwater contributions. Quat. Sci. Rev. 29, 2473–2483.
R Development Core Team, 2013. R: a language and environment for statistical computing. R foundation for statistical computing: Vienna, Austria. Computing 1, 12–21.
Reimer, P.J., Bard, E., Bayliss, A., Beck, J.W., Blackwell, P.G., Ramsey, C.B., Buck, C.E., Cheng, H., Edwards, R.L., Friedrich, M., 2013. IntCal13 and Marine13 radiocarbon age calibration curves 0–50,000 years cal BP. Radiocarbon 55, 1869–1887.
Roberts, A.P., 2015. Magnetic mineral diagenesis. Earth Sci. Rev. 151, 1–47.
Said, R., 1993. The Nile River: Geology, Hydrology, and Utilization. Vol. 320 Pergamon Press, Oxford, UK.
Stanley, D.J., Goodfriend, G.A., 1997. Recent subsidence of the northern Suez Canal. Nature 388, 335.
Stanley, J.D., Krom, M.D., Cliff, R.A., Woodward, J.C., 2003. Short contribution: Nile flow failure at the end of the Old Kingdom, Egypt: strontium isotopic and petrologic evidence. Geoarchaeology 18, 395–402.
Stueiver, M., Reimer, P.J., 1993. Extended 14C database and revised CALIB radiocarbon calibration program. Radiocarbon 28, 805–838.
Tesemma, Z., 2009. Long Term Hydrologic Trends in the Nile Basin. Cornell University Doctoral Dissertation.
Thompson, R., Oldfield, F., 1986. Environmental Magnetism. Springer, Netherlands, pp. 49–64.
Welc, F., Marks, L., 2014. Climate change at the end of the Old Kingdom in Egypt around 4200 BP: New geoarcheological evidence. Quat. Int. 324 (4), 124–133.
Wendorf, F., Schild, R., 1976. The Prehistory of the Nile Valley. Academic Press, New York, pp. 404.
Woodward, J.C., Macklin, M.G., Krom, M.D., Williams, M.A., 2007. The Nile: evolution, Quaternary river environments and material fluxes. In: Large Rivers: Geomorphology and Management, P, pp. 261–292.
Zhao, X.S., Liu, Y., Salem, A., Marks, L., Welc, F., Sun, Q.L., Jiang, J., Chen, J., Chen, Z.Y., 2017. Migration of the Intertropical Convergence Zone in North Africa during the Holocene: evidence from variations in quartz grain roundness in the lower Nile valley, Egypt. Quat. Int. 449, 22–28.